Hyperspectral Imagery Framework for Unmixing and Dimensionality Estimation*

José M.P. Nascimento[1] and José M. Bioucas-Dias[2]

[1] Instituto de Telecomunicações and Instituto Superior de Engenharia de Lisboa
R. Conselheiro Emídio Navarro, N. 1, 1959-007 Lisbon, Portugal
[2] Instituto de Telecomunicações and Instituto Superior Técnico, Technical University of Lisbon,
Av. Rovisco Pais, Torre Norte, Piso 10, 1049-001 Lisbon, Portugal
zen@isel.pt
http://www.deetc.isel.pt/jnascimento/

Abstract. In hyperspectral imagery a pixel typically consists mixture of spectral signatures of reference substances, also called endmembers. Linear spectral mixture analysis, or linear unmixing, aims at estimating the number of endmembers, their spectral signatures, and their abundance fractions.

This paper proposes a framework for hyperpsectral unmixing. A blind method (SISAL) is used for the estimation of the unknown endmember signature and their abundance fractions. This method solve a non-convex problem by a sequence of augmented Lagrangian optimizations, where the positivity constraints, forcing the spectral vectors to belong to the convex hull of the endmember signatures, are replaced by soft constraints. The proposed framework simultaneously estimates the number of endmembers present in the hyperspectral image by an algorithm based on the minimum description length (MDL) principle. Experimental results on both synthetic and real hyperspectral data demonstrate the effectiveness of the proposed algorithm.

Keywords: Blind hyperspectral unmixing, Minimum volume simplex, Minimum Description Length (MDL), Variable splitting augmented lagrangian, Dimensionality reduction.

1 Introduction

Although, there have been significant improvements in the hyperspectral sensors, there are in an image pixels that contain more than one substance, i.e., the acquired spectral vectors are mixtures of the substances spectral signatures present in the scene [6,19].

The linear mixing assumption has been widely used to describe the observed hyperspectral vectors. According to this assumption, a mixed pixel is a linear combination of endmembers signatures weighted by the corresponding abundance fractions. Due to physical considerations, the abundance fractions are subject to the so-called non-negativity and a full-additivity constraints [6].

* This work was supported by the Instituto de Telecomunicações and by the Fundação para a Ciência e Tecnologia under project HoHus (PEst-OE/EEI/LA0008/2011).

P.L. Carmona et al. (Eds.): *Pattern Recognition – Applications and Methods*, AISC 204, pp. 193–204.
DOI: 10.1007/978-3-642-36530-0_16

Hyperspectral unmixing, aims at estimating the number of reference materials, also called endmembers, their spectral signatures, and their abundance fractions [17]. Hyperspectral linear unmixing approaches can be classified as either statistical or geometrical. Statistical methods very often formulate the problem under the Bayesian framework [14] [1] [18] [21].

The geometric perspective just referred to has been exploited by many algorithms. These algorithms are based on the fact that, under the linear mixing model, hyperspectral vectors belong to a simplex set whose vertices correspond to the endmembers signatures. Thus, finding the endmembers is equivalent to identifying the vertices of the referred to simplex [20].

Some algorithms assume the presence of, at least, one pure pixel per endmember (*i.e.*, containing just one material). Some popular algorithms taking this assumption are the *pixel purity index* (PPI), [7], *vertex component analysis* (VCA), [20], the *automated morphological endmember extraction* (AMEE) [22], and the N-FINDR [26] (see [9] for recently introduced reinterpretations and improvements of N-FINDR). These methods are followed by a fully constrained least square estimation [16] or by a maximum likelihood estimation [24] of the abundance fractions to complete the unmixing procedure.

If the pure pixel assumption is not fulfilled, which is a more realistic scenario, the unmixing process is a rather challenging task, since some endmembers are not in the dataset. Some recent methods, in the vein of Craig's work *minimum Volume Transform* (MVT) [12] which finds the smallest simplex that contain the dataset, are the *simplex identification via split augmented Lagrangian* (SISAL) [4], *iterated constrained endmember* (ICE), [3], the *minimum-volume enclosing simplex algorithm* (MVES) [10], *successive volume maximization* (SVMAX) [9], and the *alternating projected subgradients* (APS) [28].

Fig. 1 illustrates three datasets raising different degrees of difficulties in what unmixing is concerned: the dataset shown in Fig.1(a) contains pure pixels, *i.e.*, the spectra corresponding to the simplex vertices are in the dataset. This is the easiest scenario with which all the unmixing algorithms cope without problems; the dataset shown in Fig.1(b) does not contain pure pixels, at least for some endmembers. This is a much more challenging, usually attacked with the minimum volume based methods, note that pure-pixels based methods are outperformed under these circumstances; Fig.1(c), contains a highly mixed dataset where only statistical methods can give accurate unmixing results.

Most of these methods assume that the number of endmembers are known a-priori or estimated for some method, such as, NWHFC [11], HySime [5], and *Second moment linear dimensionality* (SML) [2]. The *robust signal subspace estimation* (RSSE) [13] have been proposed in order to estimate the signal subspace in the presence of rare signal pixels, thus it can be used as a preprocessing step for small target detection applications. *Sparsity promoting ICE* (SPICE) [27] is an extension of ICE algorithm that incorporates sparsity-promoting priors to find the correct number of endmembers. The framework presented in [8] also estimates the number of endmembers when it unmix the data. This framework has the disadvantage of using the Unsupervised Fully Constrained Least Squares (UFCLS) algorithm proposed in [16] which assumes the presence of at least one pure pixel per endmember.

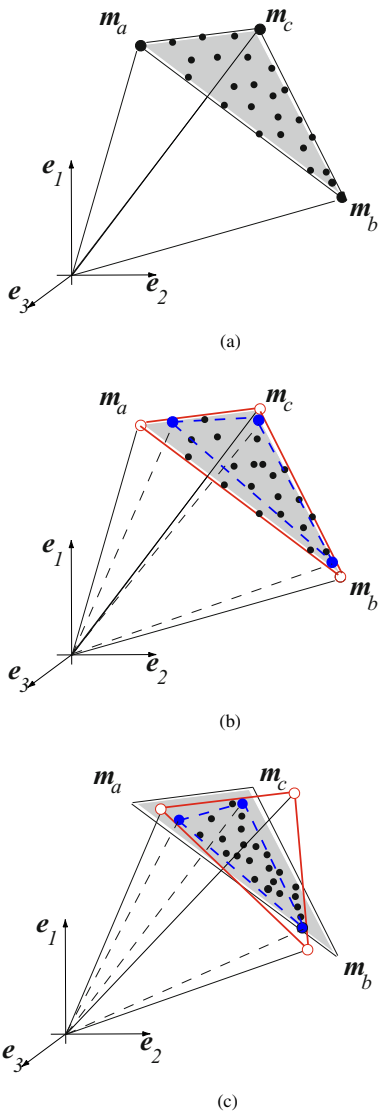

Fig. 1. Illustration of tree scenarios: (a) with pure pixels (solid line - estimated simplex by all methods); (b) without pure pixels and with pixels in the facets (solid red line - estimated simplex based on minimum volume; dashed blue line - estimated simplex by pure-pixel based methods); (c) highly mixed pixels (solid red line - estimated simplex based on minimum volume; dashed blue line - estimated simplex by pure-pixel based methods)

This paper proposes a framework for linear hyperpsectral unmixing. SISAL [4] is used for the estimation of the endmember signature and their abundance fractions, while, based on the minimum description length (MDL) principle the number of endmembers is inferred. SISAL belongs to the minimum volume class methods.

This paper is organized as follows. Section 2 formulates the problem and describes the fundamentals of the proposed method. Section 3 presents the method to infer the number of endmembers. Section 4 illustrates aspects of the performance of the proposed approach with experimental data based on U.S.G.S. laboratory spectra and with real hyperspectral data collected by the AVIRIS sensor, respectively. Section 5 concludes with some remarks.

2 Problem Formulation

Assuming the linear observation model, each pixel $\mathbf{y}$ of an hyperspectral image can be represented as a spectral vector in $\mathbb{R}^l$ (l is the number of bands) and is given by $\mathbf{y} = \mathbf{M}\mathbf{s} + \mathbf{n}$, where $\mathbf{M} \equiv [\mathbf{m}_1, \mathbf{m}_2, \ldots, \mathbf{m}_p]$ is an $l \times p$ mixing matrix ($\mathbf{m}_j$ denotes the jth endmember spectral signature), p is the number of endmembers present in the covered area, $\mathbf{s} = [s_1, s_2, \ldots, s_p]^T$ is the abundance vector containing the fractions of each endmember (notation $(\cdot)^T$ stands for vector transposed), and vector $\mathbf{n}$ holds the sensor noise and modeling errors.

To fix notation, let $\mathbf{Y} \equiv [\mathbf{y}_1, \ldots, \mathbf{y}_n] \in \mathbb{R}^{l\times n}$ denote a matrix holding the n observed spectral vectors, $\mathbf{S} \equiv [\mathbf{s}_1, \ldots, \mathbf{s}_n] \in \mathbb{R}^{p\times n}$ a matrix holding the respective abundance fractions, and $\mathbf{N} \equiv [\mathbf{n}_1, \ldots, \mathbf{n}_n] \in \mathbb{R}^{l\times n}$ accounts for additive noise. To be physically meaningful, abundance fractions are subject to non-negativity and constant sum constraints, *i.e.*, $\{\mathbf{s} \in \mathbb{R}^p : \mathbf{s} \succeq \mathbf{0}, \mathbf{1}_p^T\mathbf{s} = \mathbf{1}_n^T\}$[1]. Therefore

$$\begin{aligned} &\mathbf{Y} = \mathbf{M}\mathbf{S} + \mathbf{N} \\ \text{s.t. :} \quad &\mathbf{S} \succeq \mathbf{0}\,,\ \mathbf{1}_p^T\mathbf{S} = \mathbf{1}_n^T. \end{aligned} \tag{1}$$

Usually the number of endmembers is much lower than the number of bands ($p \ll L$). Thus, the observed spectral vectors can be projected onto the signal subspace. The identification of the signal subspace improves the SNR, allows a correct dimension reduction, and thus yields gains in computational time and complexity [5].

Let $\mathbf{E}_p$ be a matrix, with orthonormal columns, spanning the signal subspace. Thus

$$\begin{aligned} \mathbf{X} &\equiv \mathbf{E}_p^T\mathbf{Y} + \mathbf{E}_p^T\mathbf{N} \\ &= \mathbf{A}\mathbf{S} + \mathbf{N}^*, \end{aligned} \tag{2}$$

where $\mathbf{X} \equiv [\mathbf{x}_1, \ldots, \mathbf{x}_n] \in \mathbb{R}^{p\times n}$ denote a matrix holding the projected spectral vectors, $\mathbf{A} = \mathbf{E}_p^T\mathbf{M}$ is a $p \times p$ square mixing matrix, and $\mathbf{N}^*$ accounts for the projected noise.

Linear unmixing amounts to infer matrices $\mathbf{A}$ and $\mathbf{S}$. This can be achieved by fitting a minimum volume simplex to the dataset [12]. Finding a minimum volume matrix $\mathbf{A}$ subject to constraints in (1), leads to the non-convex optimization problem

$$\begin{aligned} &\widehat{\mathbf{Q}} = \arg\min_{Q} \{-\log|\det \mathbf{Q}|\} \\ \text{s.t. :} \quad &\mathbf{Q}\mathbf{X} \succeq \mathbf{0}\,,\ \mathbf{1}_p^T\mathbf{Q}\mathbf{X} = \mathbf{1}_n^T, \end{aligned} \tag{3}$$

[1] $\mathbf{s} \succeq \mathbf{0}$ means $s_j \geq 0$, for $j = 1, \ldots, p$ and $\mathbf{1}_p^T \equiv [1, \ldots, 1]$.

where $\mathbf{Q} \equiv \mathbf{A}^{-1}$. The constraint $\mathbf{1}_p^T\mathbf{Q}\mathbf{X} = \mathbf{1}_n^T$ can be simplified, by multiplying the equality on the right hand side by $\mathbf{X}^T(\mathbf{X}\mathbf{X}^T)^{-1}$, resulting $\mathbf{1}_p^T\mathbf{Q}\mathbf{X} = \mathbf{1}_n^T \Leftrightarrow \mathbf{1}_p^T\mathbf{Q} = \mathbf{a}^T$, where $\mathbf{a}^T \equiv \mathbf{1}_n^T\mathbf{X}^T(\mathbf{X}\mathbf{X}^T)^{-1}$.

SISAL aims to give a sub-optimal solution of (3) solving the following problem by a sequence of augmented Lagrangian optimizations:

$$\begin{aligned} \widehat{\mathbf{Q}}^* &= \arg\min_{Q}\{-\log|\det\mathbf{Q}| + \lambda\|\mathbf{Q}\mathbf{X}\|_h\} \\ \text{s.t. :} \quad & \mathbf{1}_p^T\mathbf{Q} = \mathbf{a}^T, \end{aligned} \tag{4}$$

where $\|\mathbf{Q}\mathbf{X}\|_h \equiv \sum_{ij} h(\mathbf{Q}\mathbf{X})$, $h(x) \equiv \max(-x, 0)$ is the so-called hinge function and λ is the regularization parameter. Notice that $\|\mathbf{Q}\mathbf{X}\|_h$ penalizes negative components of $\mathbf{Q}\mathbf{X}$, thus playing the rule of a soft constraint, yielding solutions that are robust to outliers, noise, and poor initialization.(see [4] for details).

3 Number of Endmembers Estimation

The MDL principle proposed by Rissanen [23] aims to select the model that offers the shortest description length of the data. This approach can be used to estimate the number of endmembers [8]. The well-known MDL criterion for n i.i.d. observations, in general, is given by

$$\widehat{k}_{MDL} = \arg\min_{k}\left\{\mathcal{L}(\mathbf{X}|\widehat{\boldsymbol{\theta}}_k) + \frac{1}{2}\,k\log n\right\}, \tag{5}$$

where $\mathcal{L}(\mathbf{X}|\widehat{\boldsymbol{\theta}}_k)$ is a likelihood function based on the projected data $\mathbf{X}$ with parameters $\boldsymbol{\theta}$, and $\frac{1}{2}\,k\log n$ is an increasing function penalizing higher values of k [15].

Assuming that the additive noise is Gaussian distributed, *i.e.* $\mathbf{n} \sim \mathcal{N}(0, \boldsymbol{\Lambda})$ and given a set of n i.i.d. observed samples, the likelihood equation is given by:

$$\begin{aligned} \mathcal{L}(\mathbf{X}|\widehat{\boldsymbol{\theta}}_k) &\equiv \sum_{i=1}^{n}\Big[-\log\, p(\mathbf{x}_i|\widehat{\boldsymbol{\theta}}_k)\Big] \\ &= \frac{n}{2}\Big(p\log(2\pi) + \log|\det\boldsymbol{\Lambda}|\Big) + \frac{1}{2}\mathrm{tr}\left[(\mathbf{X}-\mathbf{A}\mathbf{S})^T\,\boldsymbol{\Lambda}^{-1}\,(\mathbf{X}-\mathbf{A}\mathbf{S})\right], \end{aligned} \tag{6}$$

where $\mathrm{tr}(\cdot)$ denotes the trace of a matrix, matrices $\mathbf{A}$ and $\mathbf{S}$ are replaced by their estimates using SISAL algorithm, the noise covariance matrix, $\boldsymbol{\Lambda}$, is estimated using the algorithm based on the multiple regression theory proposed in [5] and the number of free parameters is $k = p^2$. The resulting optimization algorithm is an iterative scheme that requires to compute the objective function and to estimate the matrices $\mathbf{A}$, $\mathbf{S}$, and $\boldsymbol{\Lambda}$ for each value of p.

4 Experiments

This section provides simulated and real data experiments to illustrate the algorithm's performance. The proposed method is tested and compared with SPICE [27] on different simulated scenarios concerning with different signal-to-noise ratio (SNR), absence

of pure pixels, and number of endmembers present in the scene. The proposed method is also applied to real hyperspectral data collected by the AVIRIS sensor over Cuprite, Nevada.

4.1 Evaluation with Simulated Data

In this section the proposed method is tested on simulated scenes. To evaluate the performance of the algorithm the well-known spectral angle distance (SAD) metric is used [17]. SAD measures the shape similarity between the ith endmember signature $\mathbf{m_i}$ and its estimate $\widehat{\mathbf{m}}_i$. Based on this metric we define a spectral root mean square angle error, given by:

$$\epsilon_m \equiv \frac{1}{p}\left[\sum_{i=1}^{p}\left(\arccos\frac{\mathbf{m}_i^T\widehat{\mathbf{m}}_i}{\|\mathbf{m}_i\|\|\widehat{\mathbf{m}}_i\|}\right)^2\right]^{1/2}. \tag{7}$$

To measure the similarity between the observed data and the unmix result it is also computed the residual error between the observed pixels and their estimates:

$$r_{ls} \equiv \|\mathbf{Y} - \widehat{\mathbf{M}}\widehat{\mathbf{S}}\|_F^2, \tag{8}$$

where $\widehat{\mathbf{M}} = \mathbf{E}_p\widehat{\mathbf{A}}$ and $\widehat{\mathbf{S}}$ are estimated by SISAL.

Concerning the simulated data creation an hyperspectral image composed of 10^4 pixels is generated according to expression (1), where spectral signatures where selected from the USGS digital spectral library. The selection of endmember signatures is arbitrary as long as they are linearly independent. The reflectances contain 224 spectral bands covering wavelengths from 0.38 to $2.5\,\mu m$ with a spectral resolution of $10\,nm$. The abundance fractions are generated according to a Dirichlet distribution given by

$$D(s_1,\ldots,s_p|\mu_1,\ldots,\mu_p) = \frac{\Gamma(\sum_{j=1}^{p}\mu_j)}{\prod_{j=1}^{p}\Gamma(\mu_j)}\prod_{j=1}^{p}s_j^{\mu_j-1}. \tag{9}$$

This density, besides enforcing positivity and full additivity constraints, displays a wide range of shapes, depending on the parameters of the distribution $\boldsymbol{\mu} = [\mu_1,\ldots,\mu_p]$.

In this experiment the Dirichlet parameters are set to $\boldsymbol{\mu} = [3,\ldots,3]$, concerning the additive noise, the SNR, which is defined as

$$\text{SNR} \equiv 10\log_{10}\left(\mathbb{E}\{\mathbf{y}^T\mathbf{y}\}/\mathbb{E}\{\mathbf{n}^T\mathbf{n}\}\right), \tag{10}$$

is set to $30\,dB$.

Fig. 2 presents a scatterplot of the simulated scene for the $p = 3$ case, where dots represent the pixels and circles represent the true endmembers. This figure also shows the endmembers estimates (squares) which are very close to the true ones. Fig.3 shows the endmembers signatures (solid line) and their estimates (dashed line). Note that, in this experiment there is no pure pixels in the dataset, however, the endmembers estimate is very accurate.

Fig 4, presents the evolution of the cost function [see expression (5)] as a function of the number of endmembers. The minimum of the function occurs at $\widehat{k} = 3$ which is the true number of endmembers in the scene.

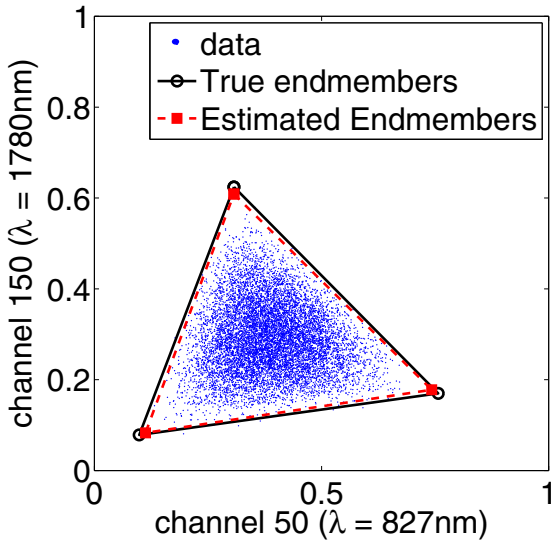

Fig. 2. Scatterplot of the three endmembers mixture: Dataset (blue dots); true endmembers (black circles); Proposed method estimates (red squares)

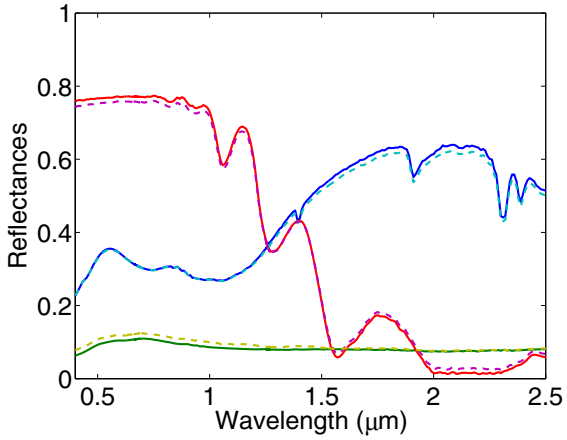

Fig. 3. Endmembers signatures (solid line) and their estimates (dashed line)

Table 1 presents the root mean square error distance ϵ_m, the residual least squares error r_{ls}, and the estimated number of endmembers for different experiments: p is set to $\{3, 5, 10\}$ and the SNR is set to $\{30, 50\}$ dB. Note that the estimated values are exactly the number of endmembers in the scene and the unmix error increases with increasing values of p and with noise level. The results achieved by SPICE in terms of residual error are similar to the proposed method results, although the errors between endmembers signatures and their estimates are worst.

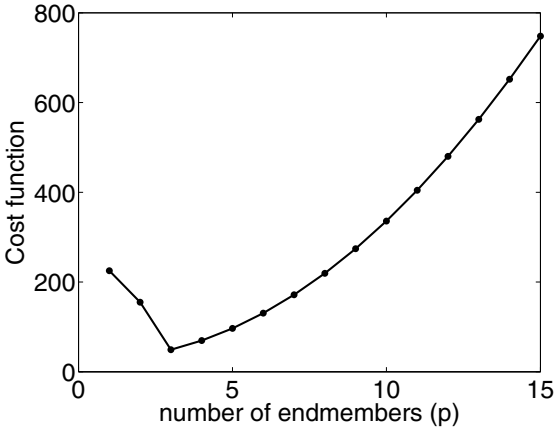

Fig. 4. Cost function evolution as a function of the number of endmembers

Table 1. Results for different scenarios as a function of the SNR and of the number of endmembers (p)

		Proposed Method			SPICE		
SNR	p	$\widehat{k}$	ϵ_m	r_{ls}	$\widehat{k}$	ϵ_m	r_{ls}
30 dB	3	3	0.048	4.76	3	0.293	4.82
	5	5	0.053	6.41	5	0.198	6.47
	10	10	0.929	6.99	6	0.258	7.18
50 dB	3	3	0.042	0.47	3	0.141	1.06
	5	5	0.059	0.64	5	0.432	1.30
	10	10	0.196	0.70	6	0.268	1.70

4.2 Experiments with Real Hyperspectral Data

In this section, the proposed method is applied to a subset (50×90 pixels and 224 bands) of the Cuprite dataset acquired by the AVIRIS sensor on June 19, 1997, Fig. 5 shows band 30 (wavelength $\lambda = 667.3nm$) of the subimage of AVIRIS cuprite Nevada dataset. The AVIRIS instrument covers the spectral region from $0.41\,\mu m$ to $2.45\,\mu m$ in 224 bands with a $10\,nm$ band width. Flying at an altitude of $20\,km$, it has an IFOV of $20\,m$ and views a swath over $10\,km$ wide. This site has been extensively used for remote sensing experiments over the past years and its geology was previously mapped in detail [25].

Table 2 present the residual error and the estimated number of endmembers for SPICE and for the proposed method. The results of both methods are comparable.

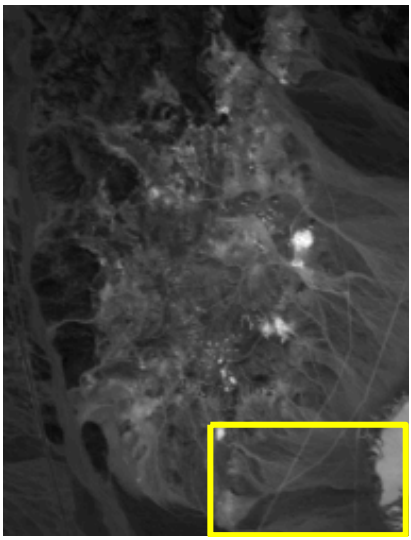

Fig. 5. Band 30 (wavelength $\lambda = 655.8nm$) of the subimage of AVIRIS Cuprite Nevada dataset (rectangle denotes the image fraction used in the experiment)

Table 2. Results for Cuprite dataset

	Proposed method	SPICE
$\widehat{k}$	6	7
r_{ls}	3.13	3.27

Fig.6 (left) shows the estimated signatures, which are compared with the nearest laboratory spectra, to visually distinguish the different endmembers an offset has been added to each signature. Note that, this endmembers are known to dominate the considered subimage [25].

Fig.6 (right) presents the estimated abundance maps for the extracted endmembers. A visual comparison show that these maps are in accordance with the known ground truth. Note that for this region Desert vanish (Fig.6b)) and Sphene (Fig. 6d)) abundance maps are very similar. These results show the potential of the proposed method to simultaneously select the number of endmembers, estimate the spectral signatures, and their abundance fractions.

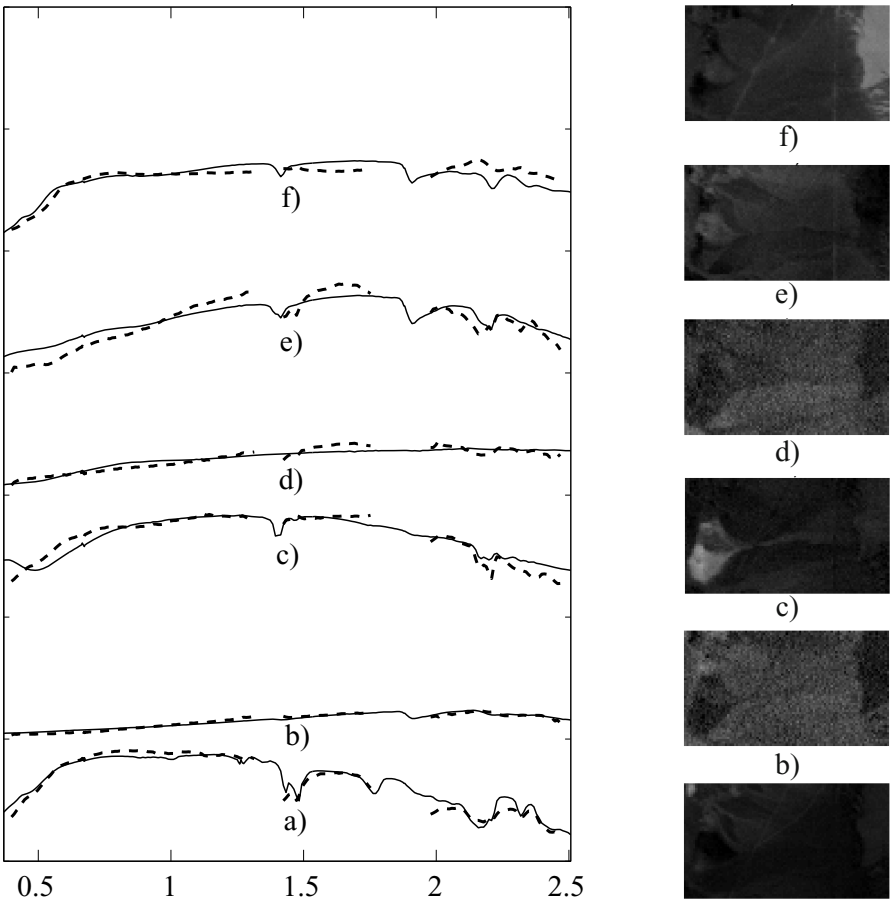

Fig. 6. Experimental results on Cuprite dataset. Left: Comparison of the estimated signatures (dashed line) with the nearest USGS spectra (solid line). Right: Abundance maps estimates. a) Alunite; b) Desert vanish; c) Dumortierite; d) Sphene; e) Kaolinite; f) Montmorillonite.

5 Conclusions

In this paper, a new framework is proposed to blindly unmix hyperspectral data and simultaneously infer the number of endmembers based on the minimum description length (MDL) principle. The estimation of the endmembers spectra and their abundance fractions is based on SISAL, which is a minimum-volume type method, that solves a non-convex problem by a sequence of augmented Lagrangian optimizations, where the positivity constraints, forcing the spectral vectors to belong to the convex hull of the endmember signatures, are replaced by soft constraints. The experimental results achieved on simulated and on real datasets show the potential of the proposed method.

References

1. Arngren, M., Schmidt, M.N., larsen, J.: Bayesian Nonnegative Matrix Factorization with Volume Prior for Unmixing of Hyperspectral Images. In: IEEE Workshop on Machine Learning for Signal Processing (MLSP) (September 2009)
2. Bajorski, P.: Second Moment Linear Dimensionality as an Alternative to Virtual Dimensionality. IEEE Trans. Geosci. Remote Sensing 49(2), 672–678 (2011)
3. Berman, M., Kiiveri, H., Lagerstrom, R., Ernst, A., Dunne, R., Huntington, J.F.: ICE: A Statistical Approach to Identifying Endmembers in Hyperspectral Images. IEEE Trans. Geosci. Remote Sensing 42(10), 2085–2095 (2004)
4. Bioucas-Dias, J.M.: A Variable Splitting Augmented Lagrangian Approach to Linear Spectral Unmixing. In: First IEEE GRSS Workshop on Hyperspectral Image and Signal Processing-WHISPERS 2009 (2009)
5. Bioucas-Dias, J.M., Nascimento, J.M.P.: Hyperspectral Subspace Identification. IEEE Trans. Geosci. Remote Sensing 46(8), 2435–2445 (2008)
6. Bioucas-Dias, J.M., Plaza, A.: Hyperspectral unmixing: geometrical, statistical, and sparse regression-based approaches, vol. 7830. SPIE (2010)
7. Boardman, J.: Automating Spectral Unmixing of AVIRIS Data using Convex Geometry Concepts. In: Summaries of the Fourth Annual JPL Airborne Geoscience Workshop, JPL Pub. 93-26, AVIRIS Workshop, vol. 1, pp. 11–14 (1993)
8. Broadwater, J., Meth, R., Chellappa, R.: Dimensionality Estimation in Hyper-spectral Imagery Using Minimum Description Length. In: Proceedings of the Army Science Conference, Orlando, FL (November 2004)
9. Chan, T.H., Ma, W.K., Ambikapathi, A., Chi, C.Y.: A simplex volume maximization framework for hyperspectral endmember extraction. IEEE Trans. Geosci. Remote Sensing 49(1), 1–17 (2011)
10. Chan, T.H., Chi, C.Y., Huang, Y.M., Ma, W.K.: A Convex Analysis-Based Minimum-Volume Enclosing Simplex Algorithm for Hyperspectral Unmixing. IEEE Trans. Signal Processing 57(11), 4418–4432 (2009)
11. Chang, C.I., Du, Q.: Estimation of Number of Spectrally Distinct Signal Sources in Hyperspectral Imagery. IEEE Trans. Geosci. Remote Sensing 42(3), 608–619 (2004)
12. Craig, M.D.: Minimum-volume Transforms for Remotely Sensed Data. IEEE Trans. Geosci. Remote Sensing 32, 99–109 (1994)
13. Diani, N.A.M., Corsini, G.: Hyperspectral Signal Subspace Identification in the Presence of Rare Signal Components. IEEE Trans. Geosci. Remote Sensing 48(4), 1940–1954 (2010)
14. Dobigeon, N., Moussaoui, S., Coulon, M., Tourneret, J.Y., Hero, A.O.: Joint Bayesian Endmember Extraction and Linear Unmixing for Hyperspectral Imagery. IEEE Trans. Signal Processing 57(11), 4355–4368 (2009)
15. Figueiredo, M.A.T., Jain, A.K.: Unsupervised Learning of Finite Mixture Models. IEEE Trans. Pattern Anal. Machine Intell. 44(3), 381–396 (2002)
16. Heinz, D., Chang, C.-I.: Fully Constrained Least Squares Linear Spectral Mixture Analysis Method for Material Quantification in Hyperspectral Imagery. IEEE Transactions on Geoscience and Remote Sensing 39(3), 529–545 (2001)
17. Keshava, N., Mustard, J.: Spectral Unmixing. IEEE Signal Processing Mag. 19(1), 44–57 (2002)
18. Moussaoui, S., Hauksdóttir, H., Schmidt, F., Jutten, C., Chanussot, J., Brie, D., Douté, S., Benediktsson, J.A.: On the Decomposition of Mars Hyperspectral Data by ICA and Bayesian Positive Source Separation. Neurocomputing 71(10-12), 2194–2208 (2008)
19. Nascimento, J.M.P., Bioucas-Dias, J.M.: Does Independent Component Analysis Play a Role in Unmixing Hyperspectral Data? IEEE Trans. Geosci. Remote Sensing 43(1), 175–187 (2005)

20. Nascimento, J.M.P., Bioucas-Dias, J.M.: Vertex Component Analysis: A Fast Algorithm to Unmix Hyperspectral Data. IEEE Trans. Geosci. Remote Sensing 43(4), 898–910 (2005)
21. Nascimento, J.M.P., Bioucas-Dias, J.M.: Hyperspectral unmixing based on mixtures of dirichlet components. IEEE Transactions on Geoscience and Remote Sensing 50(3), 863–878 (2012)
22. Plaza, A., Martinez, P., Perez, R., Plaza, J.: Spatial/Spectral Endmember Extraction by Multidimensional Morphological Operations. IEEE Trans. Geosci. Remote Sensing 40(9), 2025–2041 (2002)
23. Rissanen, J.: Modeling by Shortest Data Description. Automatica 14, 465–471 (1978)
24. Settle, J.J.: On the Relationship Between Spectral Unmixing and Subspace Projection. IEEE Trans. Geosci. Remote Sensing 34, 1045–1046 (1996)
25. Swayze, G., Clark, R., Sutley, S., Gallagher, A.: Ground-Truthing AVIRIS Mineral Mapping at Cuprite, Nevada. Summaries of the Third Annual JPL Airborne Geosciences Workshop, pp. 47–49 (1992)
26. Winter, M.E.: N-FINDR: An Algorithm for Fast Autonomous Spectral End-member Determination in Hyperspectral Data. In: Proc. of the SPIE Conference on Imaging Spectrometry, vol. 3753, pp. 266–275 (1999)
27. Zare, A., Gader, P.: Sparsity Promoting Iterated Constrained Endmember Detection in Hyperspectral Imagery. IEEE Geosci. Remote Sensing Let. 4(3), 446–450 (2007)
28. Zymnis, A., Kim, S.J., Skaf, J., Parente, M., Boyd, S.: Hyperspectral Image Unmixing via Alternating Projected Subgradients. In: 41st Asilomar Conferece on Signals, Systems, and Computer, pp. 4–7 (2007)